FINITE VOLUME MODEL FOR NONLEVEL BASIN IRRIGATION

By Scott F. Bradford[1] and Nikolaos D. Katopodes[2]

ABSTRACT: A finite volume model for unsteady, two-dimensional, shallow water flow is developed and applied to simulate the advance and infiltration of an irrigation wave in two-dimensional basins of complex topography. The fluxes are computed with Roe's approximate Riemann solver and the monotone upstream scheme for conservation laws is used in conjunction with predictor-corrector time-stepping to provide a second-order accurate solution. Flux-limiting is implemented to eliminate spurious oscillations and the model incorporates an efficient and robust scheme to capture the wetting and drying of the soil. Model predictions are compared with experimental data for one- and two-dimensional problems involving rough, impermeable, and permeable beds, including a poorly leveled basin.

INTRODUCTION

The advent of robust models for shallow-water flow has made possible the analysis and design of many complex problems in surface irrigation applications. In each of these problems, there is a large number of pertinent variables and therefore an even larger number of permutations of design and operating options. As a result, computer models have made important contributions to efficient evaluation of alternative designs in search of the optimal one. Computer simulations are much cheaper and faster than laboratory experiments and field studies, which must be adapted to different bottom conditions, geometries, and topographies. However, the modeling of surface irrigation problems is often dominated by the wetting and drying of arbitrary topography, which makes even a numerical solution difficult to obtain.

Much research has focused on developing sufficiently accurate, but computationally efficient, models because of the limited capacity and performance of computers. A number of models for surface irrigation are based on kinematic-wave or zero-inertia theory, which consist of mass and truncated forms of the momentum conservation laws (Strelkoff and Katopodes 1977; Lal 1998; Tucciarelli and Termini 2000). In kinematic-wave models, inertia and free surface slope terms are neglected, and as a result waves can only propagate downstream and are not attenuated (Katopodes 1982). Zero-inertia models retain the free surface slope and consequently allow information to propagate upstream as well (Katopodes 1982). However, the neglect of inertia precludes the accurate simulation of the flow conditions unless the Froude number is very small, typically of order 10^{-1}. Although it is possible to model the effects of ponding in one space dimension, the inability of inertialess flow to reflect waves makes it difficult to obtain satisfactory results in the presence of solid boundaries. In two space dimensions, this limitation imposes many restrictions on zero-inertia models. This is even worse for kinematic-wave models, which completely lack the ability to simulate reflective boundaries.

Computer technology has advanced sufficiently to allow for the modeling of surface irrigation with the complete two-dimensional (2D) shallow-water equations. A model based on the complete Saint-Venant equations may be applied to many similar problems, yet remains computationally feasible, unlike models based on the Navier-Stokes equations. Bradford and Katopodes (1998) presented a model that solved the 2D (longitudinal and vertical) Navier-Stokes equations coupled with Richards' equation for bed infiltration. This model is computationally intensive and would require a great deal of additional effort to extend to three dimensions, which is necessary for solving many practical problems. Fortunately, the hydrostatic approximation inherent in the shallow-water equations is sufficiently valid for most of the applications discussed here and the detail of the flow field provided by the Navier-Stokes models is not required.

Many shallow-water models have been presented in the literature, but few are applicable to problems with wetting and drying boundaries. Early tidal hydrodynamic models typically neglected the inundation of dry land by placing fixed wall boundaries near the shoreline and therefore neglect storage and energy dissipation of intermittently wetted areas. Alternatively, some models are initialized with a thin layer of water everywhere in the domain to avoid singularities caused by a zero depth (Zhang and Cundy 1989; Playán et al. 1994; Tisdale et al. 1998). However, this results in the incorrect propagation of waves since such a model will predict that a bore approaching dry land will continue through the wet/dry boundary when in actuality it should collapse and continue as a depression wave (Keller et al. 1960; Ho and Meyer 1962). The solution may also become unstable if the depth vanishes due to infiltration or flow down a slope and this approach is inefficient since the entire domain is wet and therefore the governing equations must be solved everywhere.

Several models have been developed that track wet/dry boundaries on a fixed computational grid by monitoring the wetting and drying of grid nodes and applying appropriate boundary conditions at such locations (Sielecki and Wurtele 1970; Hibberd and Peregrine 1979; Kawahara and Umetsu 1986; Casulli and Cheng 1992; Wurjanto and Kobayashi 1993; Liu et al. 1995). In addition, Wurjanto and Kobayashi (1993) applied their model to simulate seepage effects on wave runup by coupling mass and momentum equations in the permeable layer with the shallow water equations. Madsen et al. (1997) employed a different approach in which land was assigned a small porosity (even though the bed was impermeable), which allowed water to flow into the land and the intersection of the water surface and land defined the front. However, this method introduces a mass error that causes the consistent underprediction of maximum flood advance and complicates the inclusion of real bed seepage into the model.

Another group of models move the computational grid with the wet/dry interface by assuming that the nodes move with the local fluid velocity (Katopodes and Strelkoff 1978; Akanbi and Katopodes 1988; Okamoto et al. 1992; Stockstill et al. 1999). Akanbi and Katopodes (1988) also included bed seepage in their model and used the Kostiakov equation for model closure. However, moving the grid is computationally expen-

[1]Mech. Engr., Image Sci. and Applications Branch, Naval Res. Lab., Washington, DC 20375.

[2]Prof., Dept. of Civ. and Envir. Engrg., Univ. of Michigan, Ann Arbor, MI 48109.

Note. Discussion open until January 1, 2002. To extend the closing date one month, a written request must be filed with the ASCE Manager of Journals. The manuscript for this paper was submitted for review and possible publication on October 27, 2000; revised February 13, 2001. This paper is part of the ***Journal of Irrigation and Drainage Engineering***, Vol. 127, No. 4, July/August, 2001. ©ASCE, ISSN 0733-9634/01/0004-0216–0223/$8.00 + $.50 per page. Paper No. 22276.

sive since it must be regenerated each time the boundary moves and often computational nodes must be added when severe flooding occurs or removed during recession to prevent nodes from crossing and reduce grid distortion error. Titov and Synolakis (1995) developed a model that kept the wet portion of the grid fixed and added and removed grid points at the wet/dry boundary during flooding and recession, which resulted in a more efficient and robust model. However, all of the aforementioned models use finite differences, which do not conserve mass and require special front-tracking schemes to resolve discontinuities, or finite elements, which only conserve mass globally and not locally, to discretize the shallow water equations. In addition, both methods yield spurious oscillations at flow discontinuities unless first-order accurate (upwind) schemes or artificial dissipation are employed. Both approaches lead to unsatisfactory results. First-order accuracy is overly dissipative and will obscure important flow features unless a very fine grid is used. Similarly, determining the amount of artificial dissipation to use is often difficult and problem specific.

Godunov-type finite volume schemes have been utilized by many researchers for simulating shallow water flow with wetting and drying of impermeable land (Zhao et al. 1994; Fraccarollo and Toro 1995; Ambrosi 1995; and Dodd 1998). Finite volume methods are based on the integral form of the shallow-water equations, which are solved in computational cells. Therefore, mass and momentum are conserved locally, even in the presence of flow discontinuities, and arbitrary domains are easily accommodated. Fluxes are evaluated at cell faces by solving a Riemann problem, which accurately captures wave propagation and has proven to be efficient and robust. This also allows for a straightforward and efficient treatment of the dry bed problem by allowing for the flooding and drying of fixed computational cells. Also, numerical oscillations at discontinuities may be eliminated with the use of flux limiters, which have no adjustable parameters. For these reasons, a model based on a Godunov-type finite volume method for accurately simulating wetting and drying shallow water flow over a porous bed is developed and presented in this paper. The model's capabilities are illustrated through comparisons of predictions with experimental data for a variety of applications.

SHALLOW WATER EQUATIONS

The integral form of the shallow water equations form the basis of the model and are written as

$$\frac{\partial}{\partial t}\int_{\Omega} \mathbf{U}\, d\Omega + \oint_{\partial\Omega} (\mathbf{F}\, dy - \mathbf{G}\, dx) = \int_{\Omega} \mathbf{S}\, d\Omega \tag{1}$$

where $\mathbf{U} = (h \;\; hu \;\; hv)^T$ and

$$\mathbf{F} = \begin{pmatrix} hu \\ hu^2 + \frac{1}{2} gh^2 \\ huv \end{pmatrix} \tag{2}$$

$$\mathbf{G} = \begin{pmatrix} hv \\ huv \\ hv^2 + \frac{1}{2} gh^2 \end{pmatrix} \tag{3}$$

where h = flow depth; and u and v = vertically-averaged velocities in the x- and y-directions, respectively. The source terms, $\mathbf{S}$, are defined as

$$\mathbf{S} = \begin{pmatrix} -i \\ -gh\frac{\partial z}{\partial x} - c_D u\sqrt{u^2 + v^2} - \frac{ui}{2} \\ -gh\frac{\partial z}{\partial y} - c_D v\sqrt{u^2 + v^2} - \frac{vi}{2} \end{pmatrix} \tag{4}$$

where i = infiltration rate of water into the bed; z = bed elevation; and c_D bottom drag coefficient. An independent equation, typically empirical, must be utilized to determine i. Bed resistance can be described by a variety of approximations. However, availability of data in practice limits the choices to a few semiempirical equations. In this paper, the Manning equation is used to quantify bed drag, with $c_D = gn^2/h^{1/3}$. The infiltration effect on momentum conservation is an approximation given by Akanbi and Katopodes (1988).

NUMERICAL MODEL

The model is based on the model developed by Bradford and Katopodes (1999) for turbidity currents and utilizes two-step time integration for second order temporal accuracy. A predictor is computed at time level $n + 1/2$ by solving the primitive equations in generalized coordinates and a corrector is computed at the $n + 1$ time level by solving the integral equations. The primitive equations are transformed to a curvilinear coordinate system in which ξ and η are in the directions of contiguous j and k indices, respectively, while ξ_x, ξ_y, η_x, and η_y denote the grid transformation metrics from the mapping of x and y onto ξ and η, which are assumed to vary from 0 to 1 in each cell. Specifically, the equations are

$$h_{j,k}^{n+1/2} = h_{j,k}^{n} - \frac{\Delta t}{2}\left[u_\xi \overline{\Delta_\xi h} + u_\eta \overline{\Delta_\eta h} + h(\xi_x \overline{\Delta_\xi u} + \xi_y \overline{\Delta_\eta u} + \eta_x \overline{\Delta_\xi v} + \eta_y \overline{\Delta_\eta v})\right]_{j,k}^{n} \tag{5}$$

$$u_{j,k}^{n+1/2} = u_{j,k}^{n} - \frac{\Delta t}{2}\left[u_\xi \overline{\Delta_\xi u} + u_\eta \overline{\Delta_\eta u} + g(\xi_x \overline{\Delta_\xi \zeta} + \eta_x \overline{\Delta_\eta \zeta}) - c_D u\sqrt{u^2 + v^2}/h - ui/2h\right]_{j,k}^{n} \tag{6}$$

$$v_{j,k}^{n+1/2} = v_{j,k}^{n} - \frac{\Delta t}{2}\left[u_\xi \overline{\Delta_\xi v} + u_\eta \overline{\Delta_\eta v} + g(\xi_y \overline{\Delta_\xi \zeta} + \eta_y \overline{\Delta_\eta \zeta}) - c_D v\sqrt{u^2 + v^2}/h + vi/2h\right]_{j,k}^{n} \tag{7}$$

where Δt = time step; $\zeta = h + z$ = free surface elevation; $u_\xi = u\xi_x + v\xi_y$, and $u_\eta = u\eta_x + v\eta_y$. The primitive equations yield explicit values of the velocities without dividing by h, which would be necessary if solving the conservative form of the equations and therefore avoids potential numerical instability when $h \to 0$ near wet-dry boundaries. Also, the pressure and bed slope terms can be combined in this form, which eliminates problems that may arise when these terms are discretized separately.

The $\overline{\Delta}$ in (5), (6), and (7) denotes cell-average spatial gradients and are computed with a flux limiter, which preserves solution monotonicity by becoming first-order accurate near discontinuities, yet remains second-order accurate elsewhere. In this model, the Superbee limiter is used and is given by

$$\overline{\Delta u} = \begin{cases} \sin(a)\min[\max(|a|, |b|), 2\,\min(|a|, |b|)] & ab > 0 \\ 0 & ab \le 0 \end{cases} \tag{8}$$

When computing the gradients in the ξ-direction, $a = u_{j,k} - u_{j-1,k}$ and $b = u_{j+1,k} - u_{j,k}$, for example. Analogous expressions can be deduced for the gradient in the η-direction. The spatial variation of h is often much greater than the variation of ζ and computing $\overline{\Delta h}$ with a flux limiter can introduce excessive numerical dissipation into the solution (Nujić 1995). Therefore, $\overline{\Delta\zeta}$ is first computed using (8) and $\overline{\Delta h} = \overline{\Delta\zeta} - \Delta z$

is then computed. Note that Δz = nonlimited change in bed elevation in the direction of $\overline{\Delta h}$.

Predicted values to the left and right of each cell face are then reconstructed using the monotone upstream scheme for conservation laws (MUSCL) (Van Leer 1979) to achieve second-order spatial accuracy. For example, at the right (j + 1/2, k) cell face

$$u^L_{j+1/2,k} = u^{n+1/2}_{j,k} + \frac{1}{2}\,\overline{\Delta u_\xi}\Big|^n_{j,k} \tag{9}$$

$$u^R_{j+1/2,k} = u^{n+1/2}_{j+1,k} - \frac{1}{2}\,\overline{\Delta u_\xi}\Big|^n_{j+1,k} \tag{10}$$

where superscripts L and R = states to the left and right of the cell face, respectively. Similar expressions may be written for the other cell faces.

The reconstructed predictor values define a Riemann problem at each cell face, which are then used to compute the interfacial fluxes in the corrector equation

$$\frac{\mathbf{U}^{n+1}_{j,k} - \mathbf{U}^n_{j,k}}{\Delta t} + \frac{1}{\Omega_{j,k}}\left[(\mathbf{F}^{n+1/2}_\perp s)_{j+1/2,k} - (\mathbf{F}^{n+1/2}_\perp s)_{j-1/2,k} + (\mathbf{F}^{n+1/2}_\perp s)_{j,k+1/2} - (\mathbf{F}^{n+1/2}_\perp s)_{j,k-1/2}\right] = \mathbf{S}^{n+1/2}_{j,k} \tag{11}$$

where $\mathbf{U}$ and $\mathbf{S}$ are assumed to be piecewise constant in a region Ω; while $\mathbf{F}_\perp$ is assumed to be an average value on each cell face. Note also that Ω has been taken to be a quadrilateral and s is the cell face length.

The fluxes $\mathbf{F}_\perp$ are defined as

$$\mathbf{F}_\perp = \begin{pmatrix} hu_\perp \\ huu_\perp + \frac{1}{2}\,gh^2\cos\phi \\ hvu_\perp + \frac{1}{2}\,gh^2\sin\phi \end{pmatrix} \tag{12}$$

where $u_\perp$ = velocity perpendicular to the cell face; and ϕ = angle between the face normal vector and the x-axis.

The fluxes are evaluated using a Godunov-type upwind scheme in which a Riemann problem is solved across each cell face. Such methods are popular because they accurately capture waves, which is important when solving purely hyperbolic equations such as the shallow-water equations. A Riemann problem is solved utilizing the method of Roe (1981), which yields the following expression for the flux at an arbitrary cell face:

$$\tilde{\mathbf{F}}_\perp = \frac{1}{2}\,(\mathbf{F}^L_\perp + \mathbf{F}^R_\perp - \hat{\mathbf{R}}|\hat{\mathbf{\Lambda}}|\Delta\hat{\mathbf{V}}) \tag{13}$$

where $|\hat{\mathbf{\Lambda}}|$ = diagonal matrix containing the absolute values of the eigenvalues of the Jacobian of $\hat{\mathbf{F}}_\perp$

$$|\hat{\mathbf{\Lambda}}| = \begin{pmatrix} |\hat{u}_\perp - \hat{c}|^* & 0 & 0 \\ 0 & |\hat{u}_\perp| & 0 \\ 0 & 0 & |\hat{u}_\perp + \hat{c}|^* \end{pmatrix} \tag{14}$$

The asterisk denotes that these eigenvalues are modified at faces where critical flow is occurring, i.e. $-\Delta\lambda/2 < \hat{\lambda} < \Delta\lambda/2$, where λ denotes either $\hat{u}_\perp \pm \hat{c}$. This is needed because Roe's (1981) method does not yield the correct flux in this situation, which results in a shock computed within a depression wave. At such faces, these eigenvalues are computed as (Hirsch 1990)

$$|\hat{\lambda}|^* = \frac{\hat{\lambda}^2}{\Delta\lambda} + \frac{\Delta\lambda}{4} \tag{15}$$

where $\Delta\lambda = 4(\lambda^R - \lambda^L)$ yields the appropriate amount of dissipation when marching to a steady-state (Van Leer et al. 1989).

The columns of the matrix $\hat{\mathbf{R}}$ contain the corresponding right eigenvalues,

$$\hat{\mathbf{R}} = \begin{pmatrix} 1 & 0 & 1 \\ \hat{u} - \hat{a}\cos\phi & -\sin\phi & \hat{u} + \hat{a}\cos\phi \\ \hat{v} - \hat{a}\sin\phi & \cos\phi & \hat{v} + \hat{a}\sin\phi \end{pmatrix} \tag{16}$$

while the vector $\hat{\mathbf{V}}$ contains the characteristic variables, which are

$$\Delta\hat{\mathbf{V}} = \begin{bmatrix} \frac{1}{2}\left(\Delta h - \frac{\hat{h}\Delta u_\perp}{\hat{a}}\right) \\ \hat{h}\Delta u_\parallel \\ \frac{1}{2}\left(\Delta h + \frac{\hat{h}\Delta u_\perp}{\hat{a}}\right) \end{bmatrix} \tag{17}$$

where $u_\parallel$ = velocity parallel to the cell face; and Δ = finite difference across the cell face. The hat denotes a Roe (1981) average and is computed as

$$\hat{h} = \sqrt{h^L h^R} \tag{18}$$

$$\hat{u} = \frac{\sqrt{h^L}u^L + \sqrt{h^R}u^R}{\sqrt{h^L} + \sqrt{h^R}} \tag{19}$$

$$\hat{a} = \sqrt{\frac{g}{2}\,(h^L + h^R)} \tag{20}$$

The average, $\hat{v}$, is analogous to $\hat{u}$.

Hydrostatic Thrust Correction

There is a problem that results from the spatial integration of the hydrostatic thrust when computing the corrector solution with (11). The model integrates a linear function exactly, but the hydrostatic thrust varies quadratically along the cell face. Therefore a truncation error is introduced, which yields incorrect pressure forces acting on the cell. These forces generally will not balance the bed slope terms for still water on an arbitrary bottom, which initiates water motion and may result in an unstable solution. The truncation error is eliminated by analytically integrating the hydrostatic thrust to determine a correction to the approximate pressure force. For the x momentum equation this is

$$\int_s \frac{1}{2}\,gh^2\cos\phi\,ds = \frac{1}{2}\,g\cos\phi\left[h^2 + \frac{(\Delta_s h)^2}{12}\right]s \tag{21}$$

where $\Delta_s h$ = variation of h along the face. The second term on the right side of (21) is a correction term that is added to the flux computed with (13).

Source Terms

The source terms are evaluated at the cell center to maintain second-order spatial accuracy of the model. However, Bradford and Katopodes (1999) treated the bed slope source term for the x momentum equation as

$$\int_\Omega gh\,\frac{\partial z}{\partial x}\,d\Omega \approx gh\,\frac{\partial z}{\partial x}\,\Omega \tag{22}$$

where it was assumed that h and $\partial z/\partial x$ are constant within the cell. The bed slope was then computed by applying Green's theorem to convert the area integral on the left side of (22) to a cell boundary integral and then integrating z along the cell faces. Unfortunately, the assumption that h is constant yields a poor approximation of the cell body force that does not balance the pressure force for still water on a sloping bed. A more

accurate approximation to the area integral in (22) may be obtained by using finite element bilinear shape functions to represent h and z within the cell and applying 2×2 Gauss quadrature to evaluate the integral (Hughes 1987). This yields an approximation that is consistent with the corrected pressure forces and does not cause still water to spontaneously move.

Boundary Conditions

Boundary conditions are implemented by placing appropriate quantities in a ghost cell adjacent to the boundary, which defines a Riemann problem that is solved to obtain the boundary fluxes. At a supercritical inflow boundary, h, u, and v are specified in the ghost cell. If the inflow is subcritical, two quantities are specified and the remaining quantity is extrapolated from the domain adjacent to the boundary. At an outflow boundary, h, u, and v are extrapolated from the domain. At a wall, h is extrapolated and velocities are placed in the ghost cell such that $u_\perp = 0$ at the wall is zero while $u_\parallel$ is unchanged.

The methodology for tracking a wet/dry boundary has been presented and discussed by Bradford and Sanders (2001) and therefore only a brief summary is presented here. First, a depth tolerance, ε is defined such that if $h < \varepsilon$ then the momentum equations are not solved in that cell. This prevents numerical instability from arising since the volume fluxes in each cell are divided by h in order to compute u and v at the new time level. Second, cells with one to three dry corner nodes are denoted as partially filled cells and the velocities are obtained by extrapolating from the wettest neighboring cell. In such cells, the model will incorrectly estimate the pressure and body forces, which will artificially disturb quiescent water. Also, solving the integral momentum equations diffuses the wet/dry boundary since momentum is averaged over the entire cell and not just the wet portion of it. Bradford and Sanders (2001) investigated different extrapolations, but found that extrapolating the velocities from the wettest neighbor yielded sufficiently accurate results and was the most robust and efficient method for all the problems solved.

Stability Conditions

The proposed numerical scheme utilizes explicit time-stepping. Therefore, a linear stability analysis of the method indicates that the Courant condition should be observed in order to maintain the stability of the solution, which is written as

$$\left(\frac{|\lambda_\xi|}{l_\xi} + \frac{|\lambda_\eta|}{l_\eta}\right)_{\max} \Delta t \leq 1 \tag{23}$$

where λ_ξ and λ_η = eigenvalues in the ξ- and η-directions, respectively; l_ξ and l_ξ = corresponding cell length scales; and subscript "max" indicates the maximum sum of these quantities in the entire domain. However, nonlinearity of the governing equations, as well as inclusion of source terms, often act to further restrict the Courant condition (Bermudez and Vazquez 1994). When the model is stable, convergence to a unique solution is guaranteed (Sweby 1984). Convergence to steady state is also assured, when such a solution exists (Van Leer 1979).

MODEL APPLICATIONS

One-Dimensional Validation Tests

The model is first applied to simulate the flow resulting from the sudden removal of a dam in a rough impermeable channel in order to illustrate its capability to accurately predict inundation of a dry channel. The model predictions of h are compared with experimental data collected at the Waterways

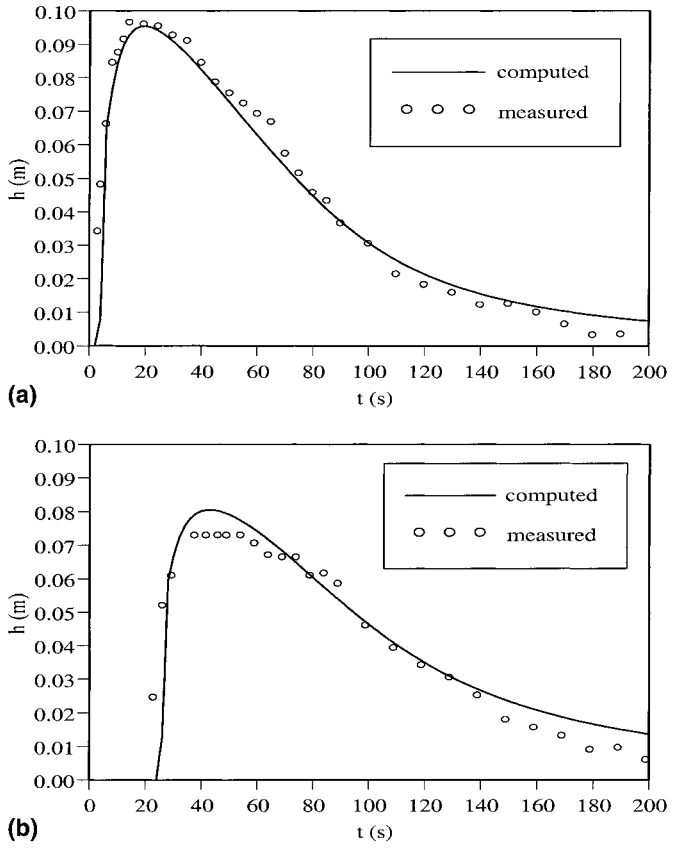

FIG. 1. Comparison of Computed and Measured Depth Hydrographs in a Smooth Channel ($n = 0.009$): (a) at 7.62 m Downstream from Dam; (b) at 45.72 m Downstream from Dam

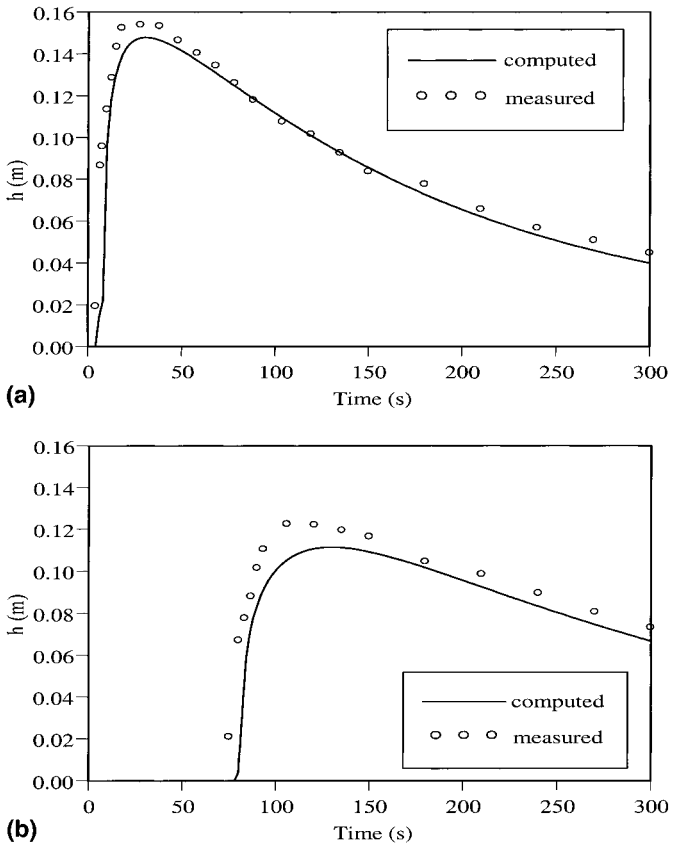

FIG. 2. Comparison of Computed and Measured Depth Hydrographs in a Rough Channel ($n = 0.05$): (a) at 7.62 m Downstream from Dam; (b) at 45.72 m Downstream from Dam

Experiment Station (Katopodes and Schamber 1983). The channel is 121.98 m long with a slope of 0.005 and there is a 0.305-m-high dam located in the middle of the channel. In the first experiment, the bed is relatively smooth with $n = 0.009$. The channel is discretized with 100 equal sized cells along the length of the channel and $\Delta t = 0.1$ s. Figs 1(a and b) show the depth hydrographs at distances of 7.62 m and 45.72 m downstream from the dam, respectively. The parameter ε was varied from 0.0001 m to 0.005 m and no effect on the solution was detected. From these figures it is seen that the model accurately predicts the arrival of the flood wave and the peak depth. Figs. 2(a and b) show the hydrographs at the same locations for a rough channel with $n = 0.05$. The model again accurately predicts the arrival of the flood wave at both locations, but it slightly underpredicts the peak depth. The model behavior in reproducing the peak of the hydrograph is characteristic of using a constant Manning n over a range of depths, especially very small depths (Katopodes and Schamber 1983). Alternative expressions for bed resistance help improve model performance, however, this was not pursued further in this paper.

The next application involves the sudden flow of water into a dry, permeable channel with bed slope equal to 0.00101. Model predictions are again compared with experimental measurements of the wave advance presented by Strelkoff and Katopodes (1977). Infiltration is treated with the Kostiakov formula

$$z_i = k\tau^a \tag{24}$$

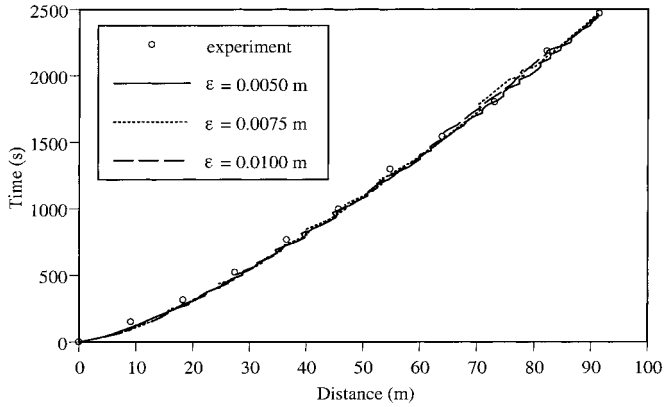

FIG. 3. Comparison of Computed and Measured Wave Advance over Permeable Bed for Varying ε

where z_i = infiltration depth; k and a = empirical constants; and τ = opportunity time for infiltration to occur. The infiltration rate is then computed as

$$i^{n+1/2} = \frac{z_i^{n+1} - z_i^n}{\Delta t} \tag{25}$$

For a typical value of Δt required for stability of the model, this is a very good approximation of the true value of $i^{n+1/2}$ and also keeps the discrete infiltration rate consistent with the infiltrated depth when a volume conservation test is performed.

The specified inflow rate is 0.00328 m^2/s, while $n = 0.024$, $k = 0.00608$ m/s^a, and $a = 0.2716$ were empirically determined (Strelkoff and Katopodes 1977). the channel is 91.44 m long and is again discretized by 100 equal size cells along the channel length and $\Delta t = 0.25$ s. Normally, the depth in each ghost cell adjacent to the inflow boundary is obtained by extrapolation from the domain and the corresponding velocities are determined by dividing the specified flow rate by the extrapolated depth. This approach works well when there is water already in the channel. However, in this problem the channel is initially dry and therefore h must be set to a nonzero value before the simulation can proceed. The choice of h is somewhat arbitrary, but it does affect the initial stability of the model. When extrapolation is not possible, h is set equal to a value just greater than the critical depth, which provides a reasonable guess. The model was not very sensitive to various initial values of h. Fig. 3 shows a comparison of experimental measurements with model predictions, which were obtained with various values of ε, for the position of the wetting front as a function of time. From the figure it is seen that agreement is quite satisfactory for all three values of ε, certainly within the error of the measurements. In addition, the results show little sensitivity to large variations in ε.

Two-Dimensional Basin Irrigation Test

A 2D test of the model involving the release of water onto a farm field is now performed. The domain is shown in Fig. 4 and water is released from a trapezoidal channel into the domain at a rate of 0.3625 m^3/s for 6,960 s. Measurements of the water surface elevation were performed at 28 locations in the domain (Al-Tamimi 1995). Since this simulation involves flood advance as well as recession, the Clemmens Branch infiltration function is implemented by fixing i to the value b during recession, i.e. for $\tau \geq t_c$ (Clemmens 1981). The empirical parameters were estimated as $k = 3.92 \times 10^{-4}$ m/s^a, a

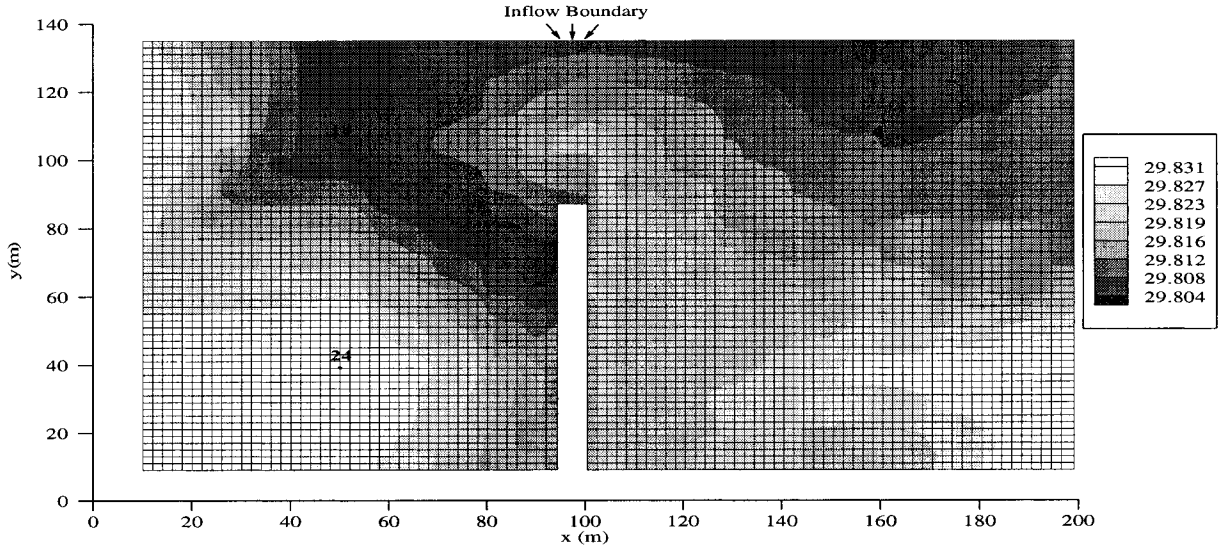

FIG. 4. Contours of Bed Elevation (in Meters) and Discretization for 2D Test Case

= 0.5, and t_c = 6,840 s from the hydrographs at all 28 stations (Al-Tamimi 1995). The domain is discretized by 5,805 cells that are uniform and square, except for the cells near the inflow boundary. All boundaries are treated as solid walls with the exception of the inflow boundary labeled in Fig. 4. The inflow boundary is 7 m wide and the flow is assumed to be subcritical with $q = 0.0518$ m^2/s and h is initially specified in the ghost cells until $h > \varepsilon$ in the domain adjacent to the boundary. For the first 60 s of simulation time, $\Delta t = 0.1$ s is used. For 60 s $< t \leq$ 6,960 s, $\Delta t = 0.5$ s is used, while for $t >$ 6,960 s, $\Delta t = 1$ s is used. In addition, $\varepsilon = 0.005$ m is specified.

Figs. 5(a and b) illustrate the resulting contours of the velocity magnitude at t = 360 s and t = 1,785, respectively. The solutions are smooth and free of spurious oscillations and yet the wetting front is sharply resolved. Fig. 6 shows the velocity vectors and contours of ζ at t = 6,960 s, at which time the inflow is stopped. At this time, the entire domain is filled with water and the solution is again free of numerical oscillations. The predicted depths at the three stations shown in Fig. 4 are compared with experimental measurements. Fig. 7(a) compares results with the measurements at station 4 and it is seen that the flood advance is well predicted. However, the agreement is less satisfactory during recession. The same trend is observed in Fig. 7(b) for station 18, as well as Fig. 7(c) for station 24. At all three locations, h is predicted to decline more rapidly than the observed depth. In order to investigate this, the value of b was examined. This value was determined from the experimental data by assuming that water level was declining at an average infiltration rate for the entire field for $\tau > t_c$ (Al-Tamimi 1995). Specifically, it was assumed that ζ was constant and advection was neglected and therefore $b \approx -\partial h/\partial t$ was assumed. However, as seen in Fig. 6, there is significant advection throughout the domain and ζ is not constant. At locations where there is a net outflow of water, b will be overestimated when neglecting advection. This is likely to occur at locations near local maxima of z, where water flows down-

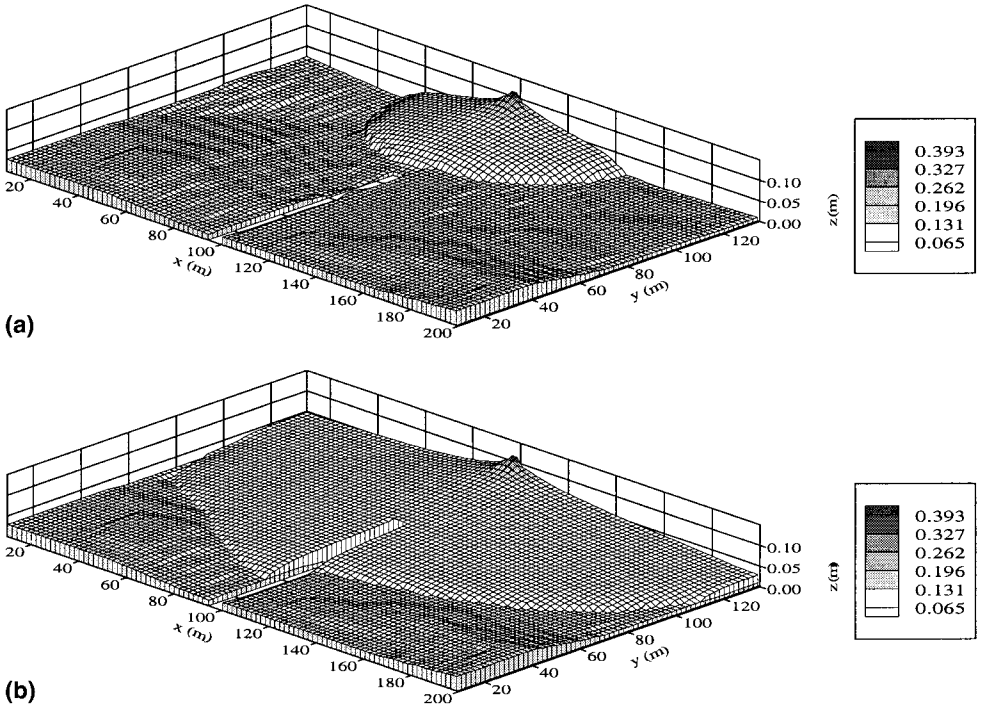

FIG. 5. Contours of h (in Meters): (a) at t = 360 s; (b) at t = 1,785 s

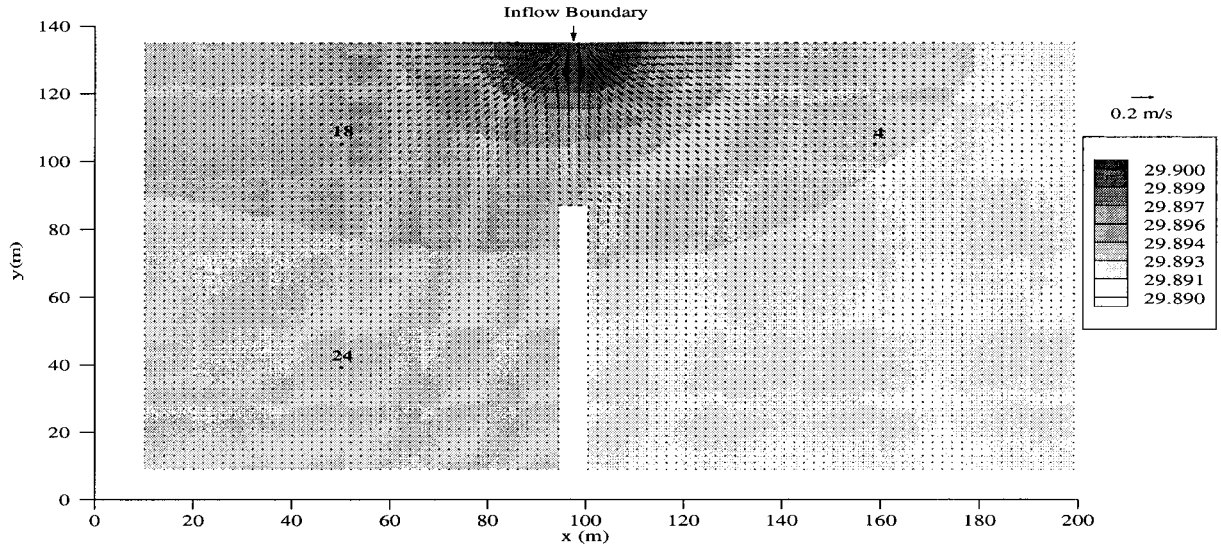

FIG. 6. Contours of h (in Meters) and Velocity Vectors at T = 6,960 s

hill and causes a rapid decline in h not related to infiltration. Station 24 is at a local peak while stations 4 and 18 are located on sloping terrain. In order to test this hypothesis, a simulation with b reduced by two orders of magnitude was performed and the results are also presented in Figs. 7(a–c). Figs. 7(a–c) show that the reduction of b yields a closer agreement between the predicted and measured hydrographs. This would seem to indicate that much of the decline in h well after the inflow is stopped is due to advection and not infiltration. However, even with a reduction in b, model agreement with observations during flood recession is not as good as in the advance stage. This is most likely due to errors in the topographic measurements, which are likely to more noticeably affect the solution during the gravity-dominated recession stage than the inertia-dominated advance stage. It is possible that b masks several other problems of the infiltration formula as well, so additional research, is needed in this direction. In addition, it may be useful to devise alternative methods for accurate estimation of b from field properties.

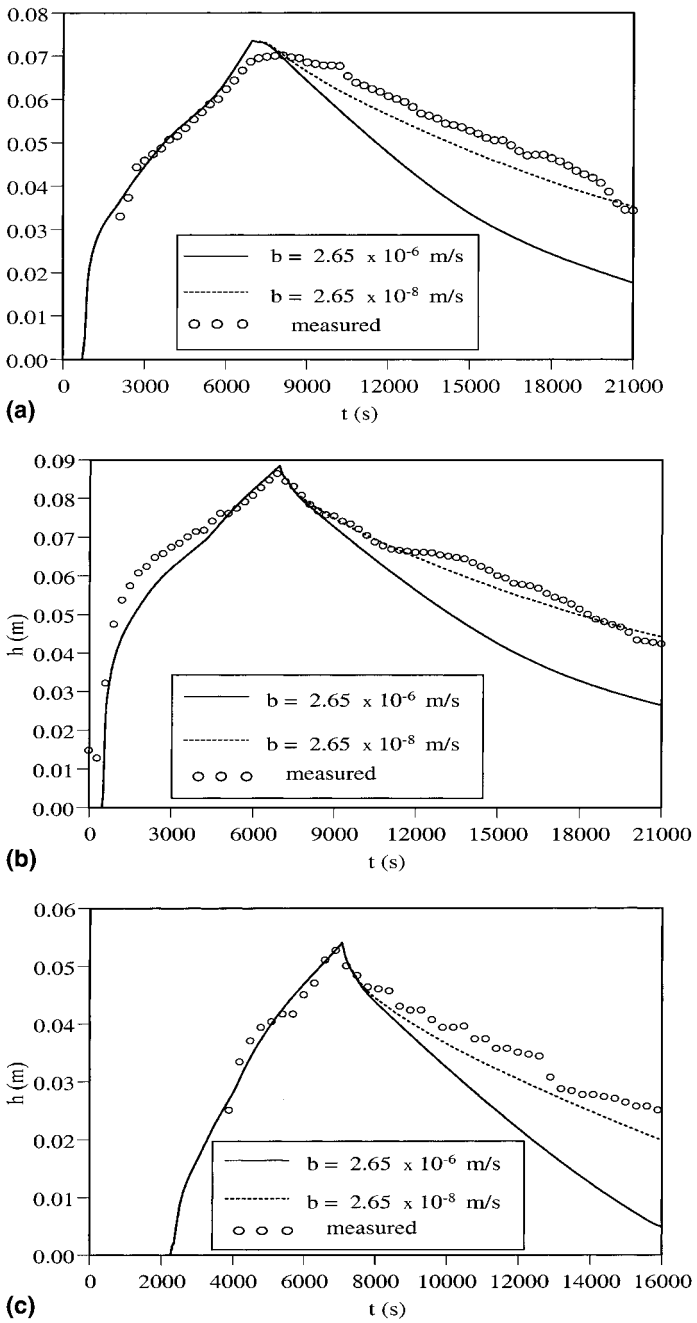

FIG. 7. Comparison of Computed and Measured Depth Hydrographs: (a) at Station 4; (b) at Station 18; (c) at Station 24

CONCLUSIONS

A robust, efficient, and accurate model for computing 2D shallow water flow over initially dry, rough, porous, arbitrary terrain has been presented. The model is based on the finite volume method, which is ideally suited for solving the shallow water equations because of its conservation properties. In addition, this method may be coupled with a Riemann solver and flux limiter to accurately capture wave motions while preventing the development of spurious oscillations that would corrupt the solution. However, the finite volume method is based on the integral form of the shallow water equations in which pressure and body forces are split into separate terms, which must be carefully discretized in order to maintain equilibrium for still water over a sloping bed.

The robustness of the model is maintained by appropriate selection of Δt as well as ε. The time step must be chosen such that the Courant condition is observed, while ε may vary depending on the specific problem. In particular, problems with greater bed drag and infiltration require larger values of ε for a given Δt, but ε should be kept as small as possible in order to limit its effect on the solution. It was shown, however, that ε can be varied over a large range of values without significantly altering the solution. Generally, a value $\varepsilon = 0.005$ m has been found to be sufficient for most surface irrigation applications.

The model's efficiency is due to the use of explicit time integration, which does not require the inversion of large matrices as do implicit schemes. The use of explicit time stepping requires the observance of the Courant condition, which is not required with implicit methods. However, the Courant condition must also be obeyed in order to compute accurate, transient solutions of the shallow water equations, which negates the advantage of implicit schemes. This is particularly true for problems with moving wet/dry fronts. Therefore, explicit methods are the more efficient schemes for this study.

The accuracy of the model was demonstrated by favorable comparisons with experimental measurements for 1D and 2D problems including the dam-break problem as well as flow in an irrigation basin. In addition, some of the difficulties associated with modeling seepage outflow were addressed. The proposed model is quite general and may also be applied to model floodplain inundation and wave runup with no additional modifications other than appropriate boundary conditions.

REFERENCES

Akanbi, A. A., and Katopodes, N. D. (1988). "Model for flood propagation on initially dry land." *J. Hydr. Engrg.*, ASCE, 114(7), 689–706.

Al-Tamimi, A. H. J. (1995). "Two-dimensional transient flow in non-level basins." PhD dissertation, Dept. of Agric. and Biosys. Engrg., University of Arizona, Tucson, Ariz.

Ambrosi, D. (1995). "Approximation of shallow water equations by Roe's Riemann solver." *Int. J. Numer. Methods in Fluids*, 20, 157–168.

Bermudez, A., and Vazquez, M. E. (1994). "Upwind methods for hyperbolic conservation laws with source terms." *Comp. and Fluids*, 23, 1049–1071.

Bradford, S. F., and Katopodes, N. D. (1998). "Nonhydrostatic model for surface irrigation." *J. Irrig. and Drain. Engrg.*, ASCE, 124(4), 200–212.

Bradford, S. F., and Katopodes, N. D. (1999). "Hydrodynamics of turbid underflows. I: Formulation and numerical analysis." *J. Hydr. Engrg.*, ASCE, 125(10), 1006–1015.

Bradford, S. F., and Sanders, B. F. (2001). "Finite volume model for shallow water flooding and drying of arbitrary topography." *J. Hydr. Engrg.*, ASCE, in press.

Casulli, V., and Cheng, R. T. (1992). "Semi-implicit finite difference

methods for three-dimensional shallow water flow." *Int. J. Numer. Methods in Fluids*, 15, 629–648.
Clemmens, A. J. (1981). "Evaluation of infiltration measurements for border irrigation." *Agric. Water Mgmt.*, 3, 251–267.
Dodd, N. (1998). "Numerical model of wave run-up, overtopping, and regeneration." *J. Wtrwy., Port, Coast., and Oc. Engrg.*, ASCE, 124(2), 73–81.
Fraccarollo, L., and Toro, E. F. (1995). "Experimental and numerical assessment of the shallow water model for two-dimensional dam-break type problems." *J. Hydr. Res.*, 33, 843–864.
Hirsch, C. (1990). Numerical computation of internal and external flows, Wiley, New York.
Ho, D. V., and Meyer, R. E. (1962). "Climb of a bore on beach." *J. Fluid Mech.*, 14, 305–318.
Hughes, T. J. R. (1987). *The finite element method*, Prentice-Hall, Englewood Cliffs, N.J.
Katopodes, N. D. (1982). "On zero-inertia and kinematic waves." *J. Hydr. Div.*, ASCE, 108(11), 1380–1387.
Katopodes, N., and Schamber, D. R. (1983). "Applicability of dam-break flood wave models." *J. Hydr. Engrg.*, ASCE, 109(5), 702–721.
Katopodes, N. D., and Strelkoff, T. (1977). "Dimensionless solutions of border-irrigation advance." *J. Irrig. and Drain. Div.*, ASCE, 103(4), 401–417.
Katopodes, N., and Strelkoff, T. (1978). "Computing two-dimensional dam-break flood waves." *J. Hydr. Div.*, ASCE, 104(9), 1269–1288.
Kawahara, M., and Umetsu, T. (1986). "Finite element method for moving boundary problems in river flow." *Int. J. Numer. Methods in Fluids*, 6, 365–386.
Keller, H. G., Levine, D. A., and Whitham, G. B. (1960). "Motion of a bore over a sloping beach." *J. Fluid Mech.*, 7, 302–316.
Lal, A. M. W. (1998). "Weighted implicit finite-volume model for overland flow." *J. Hydr. Engrg.*, ASCE, 124(9), 941–950.
Liu, P. L. F., Cho, Y., Briggs, M. J., Kanoglu, U., and Synolakis, C. E. (1995). "Runup of solitary waves on a circular island." *J. Fluid Mech.*, 302, 259–285.
Madsen, P. A., Sorensen, O. R., and Schaffer, H. A. (1997). "Surf zone dynamics simulated by a Boussinesq type model. Part I. model description and cross-shore motion of regular waves." *Coast. Engrg.*, 32, 255–287.
Nujić, M. (1995). "Efficient implementation of non-oscillatory schemes for the computation of free-surface flows." *J. Hydr. Res.*, 33, 101–111.
Okamoto, T., Kawahara, M., Ioki, N., and Nagaoka, H. (1992). "Two-dimensional wave run-up analysis by selective lumping finite element method." *Int. J. Numer. Methods in Fluids*, 14, 1219–1243.
Playán, E., Walker, W. R., and Merkley, G. P. (1994). "Two-dimensional simulation of basin irrigation. I: Theory," *J. Irrig. and Drain. Engrg.*, ASCE, 120(5), 837–856.
Roe, P. L. (1981). "Approximate Riemann solvers, parameter vectors, and difference schemes." *J. Computational Physics*, 43, 357–372.
Sielecki, A., and Wurtele, M. G. (1970). "The numerical integration of the nonlinear shallow-water equations with sloping boundaries." *J. Computational Physics*, 6, 219–236.
Stockstill, R. L., Berger, R. C., and Nece, R. E. (1997). "Two-dimensional flow model for trapezoidal high-velocity channels." *J. Hydr. Engrg.*, ASCE, 123(10), 844–852.
Strelkoff, T., and Katopodes, N. D. (1977). "Border-irrigation hydraulics with zero inertia." *J. Irrig. and Drain. Div.*, ASCE, 103(3), 325–342.
Sweby, P. K. (1984). "High resolution schemes using flux limiters for hyperbolic conservation laws." *SIAM J. of Numer. Anal.*, 21, 995–1011.
Titov, V. V., and Synolakis, C. E. (1995). "Modeling of breaking and nonbreaking long-wave evolution and runup using VTCS-2." *J. Wtrwy., Port, Coast., and Oc. Engrg.*, ASCE, 121(6), 308–316.
Tisdale, T. S., Scarlatos, P. D., and Hamrick, J. M. (1998). "Streamline upwind finite-element method for overland flow." *J. Hydr. Engrg.*, ASCE, 124(4), 350–357.
Tucciarelli, T., and Termini, D. (2000). "Finite-element modeling of floodplain flow." *J. Hydr. Engrg.*, ASCE, 126(6), 416–424.
Van Leer, B. (1979). "Towards the ultimate conservative difference scheme. V. A second order sequel to Godunov's method." *J. Computational Physics*, 32, 101–136.
Van Leer, B., Lee, W. T., and Powell, K. G. (1989). "Sonic point capturing." *AIAA 9th Computational Fluid Dynamics Conf.*, Buffalo, N.Y.
Wurjanto, A., and Kobayashi, N. (1993). "Irregular wave reflection and runup on permeable slopes." *J. Wtrwy., Port, Coast., and Oc. Engrg.*, ASCE, 119(5), 537–557.
Zhang, W., and Cundy, T. W. (1989). "Modeling of two-dimensional overland flow." *Water Resour. Res.*, 25, 2019–2035.
Zhao, D. H., Shen, H. W., Tabios, G. Q., III, Lai, J. S., and Tan, W. Y. (1994). "Finite-volume two-dimensional unsteady-flow model for river basins." *J. Hydr. Engrg.*, ASCE, 120(7), 863–883.

NOTATION

The following symbols are used in this paper:

c = celerity of simple gravity wave;
$\mathbf{F}_\perp$ = vector of fluxes perpendicular to cell face;
g = acceleration due to gravity;
h = flow depth;
i = bed infiltration rate;
$\mathbf{R}$ = matrix of right eigenvectors of Jacobian of $\mathbf{F}_\perp$;
$\mathbf{S}$ = vector of conservative source terms;
t = temporal coordinate;
u = vertically averaged velocity in x-direction;
$\mathbf{U}$ = vector of conservative variables;
$u_\perp$ = vertically averaged velocity perpendicular to cell face;
$\mathbf{V}$ = vector of characteristic variables;
v = vertically averaged velocity in y-direction;
x = spatial coordinate;
y = spatial coordinate;
z = bed elevation from arbitrary datum;
z_i = infiltration depth;
$\mathbf{\Delta}$ = jump in flow property across discontinuity;
ε = depth tolerance;
$\mathbf{\Lambda}$ = diagonal matrix of eigenvalues of Jacobian of $\mathbf{F}_\perp$; and
λ = individual eigenvalues of Jacobian of $\mathbf{F}_\perp$.